Monthly Notices
of the
ROYAL ASTRONOMICAL SOCIETY

MNRAS **454,** 531–540 (2015) doi:10.1093/mnras/stv1987

Spectroscopic constraints on CH_3OH formation: CO mixed with CH_3OH ices towards young stellar objects

E. M. Penteado,[1⋆] A. C. A. Boogert,[2] K. M. Pontoppidan,[3] S. Ioppolo,[4] G. A. Blake[5] and H. M. Cuppen[1⋆]

[1]*Institute for Molecules and Materials, Radboud University, Heyendaalsweg 135, NL-6525 AJ Nijmegen, the Netherlands*
[2]*Universities Space Research Association, Stratospheric Observatory for Infrared Astronomy, NASA Ames Research Center, MS 232-11, Moffett Field, CA 94035, USA*
[3]*Space Telescope Science Institute, 3700 San Martin Drive, Baltimore, MD 21218, USA*
[4]*Department of Physical Sciences, The Open University, Walton Hall, Milton Keynes MK7 6AA, UK*
[5]*Division of Geological & Planetary Sciences, California Institute of Technology, Mail Stop 150-21, Pasadena, CA 91125, USA*

Accepted 2015 August 21. Received 2015 August 21; in original form 2015 July 17

ABSTRACT

The prominent infrared absorption band of solid CO – commonly observed towards young stellar objects (YSOs) – consists of three empirically determined components. The broad 'red component' (2136 cm^{-1}, 4.681 μm) is generally attributed to solid CO mixed in a hydrogen-bonded environment. Usually, CO embedded in the abundantly present water is considered. However, CO:H_2O mixtures cannot reproduce the width and position of the observed red component without producing a shoulder at 2152 cm^{-1}, which is not observed in astronomical spectra. Cuppen et al. showed that CO:CH_3OH mixtures do not suffer from this problem. Here, this proposition is expanded by comparing literature laboratory spectra of different CO-containing ice mixtures to high-resolution ($R = \lambda/\Delta\lambda = 25\,000$) spectra of the massive YSO AFGL 7009S and of the low-mass YSO L1489 IRS. The previously unpublished spectrum of AFGL 7009S shows a wide band of solid ^{13}CO, the first detection of ^{13}CO ice in the polar phase. In this source, both the ^{12}CO and ^{13}CO ice bands are well fitted with CO:CH_3OH mixtures, while respecting the profiles and depths of the methanol bands at other wavelengths, whereas mixtures with H_2O cannot. The presence of a gradient in the CO:CH_3OH mixing ratio in the grain mantles is also suggested. Towards L1489 IRS, the profile of the ^{12}CO band is also better fitted with CH_3OH-containing ices, although the CH_3OH abundance needed is a factor of 2.4 above previous measurements. Overall, however, the results are reasonably consistent with models and experiments about formation of CH_3OH by the hydrogenation of CO ices.

Key words: astrochemistry – stars: formation – stars: individual: L1489 IRS, AFGL 7009S – ISM: abundances – ISM: molecules – infrared: ISM.

1 INTRODUCTION

The absorption profile of interstellar solid CO around 2140 cm^{-1} has proven to be a great source of information about the chemical composition, structure, and evolution of interstellar ices (Tielens et al. 1991). As described by Pontoppidan et al. (2003), this prominent feature can be decomposed into different components: a broad component peaking at 2136.5 cm^{-1}, named the red component, and two other narrower features peaking at 2139.7 and 2143.7 cm^{-1}, called the middle and blue components, respectively. According to these authors, the physical explanation for this decomposition is that solid CO resides in a maximum of three molecular environments. Comparisons between laboratory-based infrared spectra of ice analogues and observations of ice sources towards young stellar object (YSO) have been used to identify the molecular environment responsible for the observed absorption features and to characterize the chemical and physical properties of the environments where the ices are found.

The middle component has been attributed to CO in an apolar environment, like pure CO, while the blue component has been attributed to CO mixed with other apolar species, such as CO_2, N_2, or O_2. In view of the high cosmic abundance of N and O, and the fact that their desorption temperature is similar to that of CO (Öberg et al. 2005; Acharyya et al. 2007), these species might easily be mixed with CO in the ice (Elsila, Allamandola & Sandford 1997). The red component, on the other hand, has been explained as being caused by CO mixed with some polar species (i.e. CO in a hydrogen-bonded environment). Since water is the main species

⋆ E-mail: e.monfardini@science.ru.nl (EMP); H.Cuppen@science.ru.nl (HMC)

present in ice mantles, it was mainly considered as the species responsible for this component (Sandford et al. 1988; Tielens et al. 1991). However, discrepancies between observed and laboratory infrared spectra of ice analogues has raised doubts about H_2O and CO mixtures in ice mantles. Although experiments have shown the presence of a shoulder at 2152 cm^{-1} due to the interaction of CO with dangling OH bonds in amorphous ice when CO is mixed with H_2O, such a feature has never been observed. Therefore, observational issues have been suggested as explanation for the non-detection of the 2152 cm^{-1} absorption band. The spectral features from other species equally present in the ice, for instance the CN stretch vibrational mode at 2165 cm^{-1}, could hide the 2152 cm^{-1} band (Schmitt, Greenberg & Grim 1989) or the lack of sufficient resolution could prevent the spectrum to be sufficiently resolved in this range (Sandford et al. 1988; Ehrenfreund et al. 1997). Pontoppidan et al. (2003) showed indisputably in a higher resolution observational study that the 2152 cm^{-1} band is not present in any line of sight towards 39 YSOs. An explanation based on the chemistry of ices was then suggested by Fraser et al. (2004). These authors proposed that the 2152 cm^{-1} band is suppressed by the interaction of CO with dangling OH at the interface between CO and H_2O in layered ices. However, the presence of the red component cannot be explained by this supposition. Therefore, in addition to the layering hypothesis, Fraser et al. (2004) proposed that the presence of species like CH_3OH or CO_2 could block the dangling OH which, in turn, would eliminate the 2152 cm^{-1} band from astronomical spectra.

Unlike CO:H_2O ices, laboratory mixtures of CO and methanol, the second most abundant polar molecule in interstellar ices, do not present a shoulder at 2152 cm^{-1}. Moreover, since methanol has been shown to be the final product of the hydrogenation of CO ice, methanol could potentially be a good candidate for the red component. With this in mind, we recently published a study (Cuppen et al. 2011) in which the widths and positions of infrared laboratory spectra of CO:CH_3OH ice mixtures were compared with those of the red component of the aforementioned survey by Pontoppidan et al. (2003). This comparison showed that the observed spectral characteristics correspond to the characteristics of laboratory spectra of CO:CH_3OH mixtures with ratios between 1:9 and 9:1. On the basis of these results, we concluded that this provides extra evidence that the ice mantle is likely composed of separate H_2O- and CO-rich layers, in which the latter is mixed with CH_3OH in different mixing ratios. Here we take the proposition that the red component is due to CO+CH_3OH in an intimate mixture further to the test. This is a polar environment, not unlike that of H_2O, similarly giving rise to a broad, redshifted band compared to that of pure CO or CO in an apolar environment. This is supported by models which show that CH_3OH can be formed by hydrogenation of CO ice. Furthermore, H_2O:CO:CO_2 mixtures of different ratios and temperatures were also tested by Cuppen et al. (2011) and the conclusion was that such mixtures can indeed suppress the 2152 cm^{-1} feature, but (1) the amount of CO_2 needed for that is unrealistic, and the spectral characteristics of the red component cannot be properly reproduced, and (2) more realistic ratios can make the 2152 cm^{-1} feature weaker only for annealed ices. However, Cuppen et al. (2011) did not consider the shape and depths of the CH_3OH and H_2O bands, nor did they consider grain shape effects. As pointed out by Tielens et al. (1991), grain shape can induce changes in the profiles of ice mixtures which contain CO in a high concentration. In the present paper, shape effects are taken into account by correcting the laboratory spectra following a Continuous Distribution of Ellipsoids (CDE) model as described by Bohren & Huffman (1983).

Here, we present a high-resolution, high signal-to-noise ratio spectrum of the high-mass YSO AFGL 7009S. This source presents a prominent red component in the solid CO band, indicating a high abundance of polar species mixed with CO. To test the methanol-in-CO hypothesis, we not only consider the CO band but also different methanol bands of AFGL 7009S, to further constrain the results. These are necessary constraints to justify the presence of methanol in the ice mantle. Therefore, here we focus on CO:CH_3OH mixtures to reproduce the red component, and give only one example of CO:H_2O mixture to illustrate the mismatch of such mixture with observations. We also present the detection of solid ^{13}CO in AFGL 7009S in addition to ^{12}CO. The first detection of solid ^{13}CO in the interstellar medium was reported by Boogert, Blake & Tielens (2002b). This band is a tracer for the ice composition, since its characteristics and position do not depend on grain shape effects due to the low concentration of ^{13}CO. The ^{12}CO band is broader than the ^{13}CO band, which reflects the potential effect that grain shape effects have on the feature of the ^{12}CO band (Boogert et al. 2002b).

The same fitting procedure is also applied to the low-mass YSO L1489 IRS. This source also shows a salience at long wavelengths of the CO feature, and the detection of CH_3OH has also been reported (Boogert, Hogerheijde & Blake 2002a; Boogert et al. 2008), but with lower abundance. Although we work with a smaller sample than Cuppen et al. (2011), the present study includes new details, such as grain shape corrections and direct comparison between laboratory and observed spectra. The latter are taken at much higher resolution than the observations used in the earlier study.

The present paper is structured as follows: the observations of the YSOs are described in Section 2 and the laboratory spectra are presented in Section 3. The fitting procedure is described in Section 4, including briefly the method to extract the optical constants from the laboratory spectra (Section 4.1), the method of correction for grain shape effects (Section 4.2), and a description of the ice components and the constraints (Section 4.3). The results are presented in Section 5. In Section 6 we present a discussion and the astrophysical implications of our results.

2 OBSERVATIONS

The vibrational modes of solid ^{12}CO and ^{13}CO were observed at high resolution ($R = \lambda/\Delta\lambda = 25\,000$) towards the low-mass YSO L1489 IRS and the massive YSO AFGL 7009 S obtained with the near-infrared echelle spectrograph (NIRSPEC) spectrometer (McLean et al. 1998) at the Keck II telescope. The spectrum of L1489 IRS covers the wavelength range of 4.615–4.819 μm and was first published in Boogert et al. (2002a). We refer to that work for details about the data reduction procedure. The final, unsmoothed signal-to-noise ratio is ∼45, and regions with less than 50 per cent of the maximum atmospheric transmission were removed from the data. The *M*-band spectrum of AFGL 7009 S was obtained on 2003 July 11, covering the wavelength ranges of 4.648–4.720 and 4.763–4.830 μm, at airmasses of 1.33 and 1.18, respectively. Telluric absorption lines were divided out using the standard star HR 7950 (B9.5 V). The data reduction procedures applied were the same as for L1489 IRS. The final signal-to-noise ratio in the unsmoothed spectra is ∼100 and 300 in the 4.648–4.720 and 4.763–4.830 μm ranges, respectively.

The vibrational modes of H_2O and CH_3OH were studied in wide-band spectra of L1489 IRS and AFGL 7009S, previously published in Boogert et al. (2008). The *L*-band spectrum of L1489 IRS (2.85–4.15 μm), obtained with Keck/NIRSPEC at Keck II, has a resolution

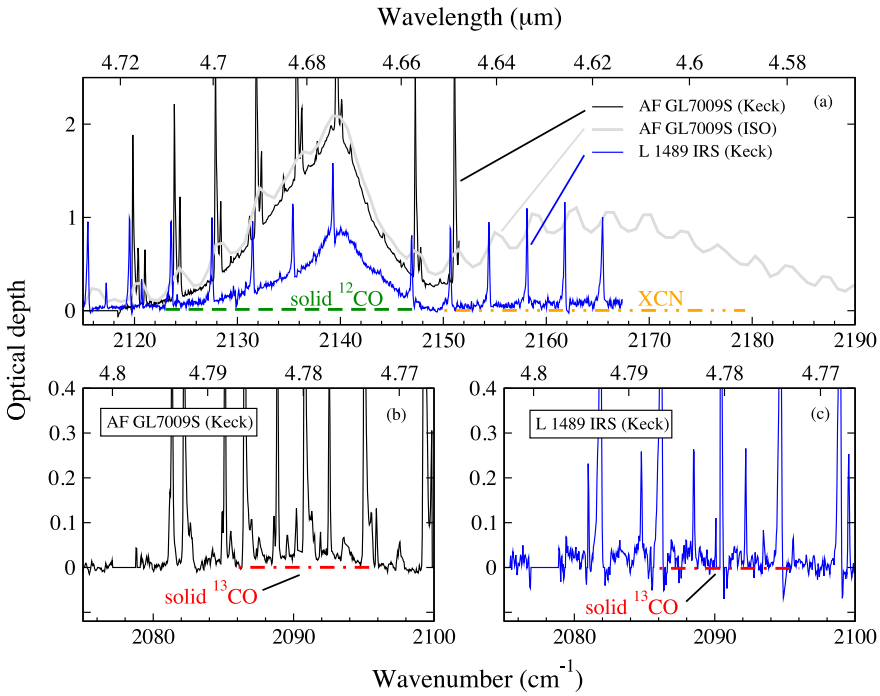

Figure 1. Observed high-resolution ($R = 25\,000$) Keck spectrum of AFGL 7009S (black) and L1489 IRS (blue). (a) Solid ^{12}CO (green dashed line) and XCN (orange double-dots dashed line) spectral ranges are highlighted. Observation of AFGL 7009S with ISO (grey, lower resolution, $R \sim 400$) show a strong feature in the XCN band, which is not seen in the L1489 IRS spectrum. (b) ^{13}CO band (spectral range highlighted in red dot–dashed line) of AFGL 7009S observed with Keck. (c) Same as (b) but for L1489 IRS, for which no ^{13}CO ice band was detected. Deepest narrow lines in all panels are caused by gas-phase CO. (A colour version of this figure is available in the online version.)

of $R \sim 2000$. The spectrum above 5.3 μm was obtained with the Infrared Spectrometer (IRS) at the *Spitzer* Space Telescope at a resolving power of $R \sim 60$–120 in the 5.3–10 μm range, and $R \sim 600$ at longer wavelengths. The spectrum of AFGL 7009 S was obtained with the Short Wavelength Spectrometer (SWS) on board the Infrared Space Observatory (ISO) in SWS01, speed 3, mode, covering the wavelength range of 2.3–40 μm at a resolving power of $R \sim 400$.

The ISO spectrum of AFGL 7009 S was scaled to the Keck spectrum to obtain a larger baseline for the absorption features. The observation covering the 3.45–4 μm range of AFGL 7009 S was taken from Dartois et al. (1999) (obtained with United Kingdom Infrared Telescope) and the reader is guided to this reference for details. Finally, the high-resolution spectra of ^{13}CO and ^{12}CO bands of both sources are shown in Fig. 1, as well as the lower resolution ISO spectrum of the XCN band of AFGL 7009 S.

3 EXPERIMENTAL SPECTRA

All laboratory spectra are obtained from standard experimental procedures and were not measured as part of this paper. Experiments with all mixtures were performed at the *Sackler Laboratory for Astrophysics*, Leiden University, Netherlands, except for CO:O_2:N_2:CO_2 = 1:5:1:0.5, which was performed at the NASA Ames Research Center, CA, USA. The CO:CH_3OH spectra are taken from Cuppen et al. (2011). The mixtures CO:CH_3OH = 9:1 and 4:1 are saturated. Therefore, those mixtures are not used here. Pure CO, CO:H_2O, and CO:O_2:N_2:CO_2 = 1:0.5:0.25:0.32 spectra are taken from Ehrenfreund et al. (1996) and CO:O_2:N_2:CO_2 = 1:5:1:0.5 spectrum is taken from Elsila et al. (1997). Details about the laboratory ices used here are summarized in Table 1.

4 FITTING PROCEDURE

When comparing interstellar spectra with laboratory spectra, the size and shape of the interstellar grains must be taken into account. For grains smaller compared to the wavelength, i.e. in the Rayleigh limit ($2\pi a/\lambda \ll 1$), grain shapes start to play a role. In this regime, the polarization of the grains by the electromagnetic radiation leads to resonances with the molecular dipoles, which changes the profile and peak position of the ice absorption bands. To calculate grain shape corrected spectra, optical constants are needed. Therefore, the fitting procedure involves several steps: first the optical constants are extracted from the laboratory data; these are then applied to generate the grain shape corrected spectra which are used to fit the spectra observed towards YSOs.

4.1 Optical constants

The optical constants are the real (n) and the imaginary (k) parts of the total complex refractive index $\boldsymbol{n}$, where ($\boldsymbol{n} = n + ik$). These were determined by using a Kramers–Kronig analysis of the infrared laboratory spectra following Hudgins et al. (1993).[1] The values of n_0 (optical refractive index) used here are equal to Hudgins et al. (1993): $n_0 = 1.30$ for pure CO and CO-dominated ices, $n_0 = 1.33$ for ices dominated by CH_3OH, and $n_0 = 1.32$ for H_2O-rich ices. For ices with the same ratio of CO and CH_3OH, we used the average of $n_0 = 1.315$. The ice thickness h is estimated through the depth of the ice features using the band strengths, 1.2×10^{-16}, 1.0×10^{-17}, and 4.9×10^{-18} cm molec^{-1} (Grim et al. 1991) for the 3247,

[1] Note that in equation (5) of Hudgins et al. (1993) the term 1/h should multiply the remainder of the equation.

Table 1. Laboratory ices used in this work.

Ice composition	Ratio	Temperature (K)	Spectral range (cm^{-1})	Resolution (cm^{-1})	Thickness (μm)	n_0	Reference	Used in figure
$CO:CH_3OH$	2:1	15	400–4000	1	0.32	1.30	1	2
$CO:CH_3OH$	1:1	15	400–4000	1	0.25	1.315	1	3, 5, 8
$CO:CH_3OH$	1:2	15	400–4000	1	0.12	1.33	1	5, 8
$CO:CH_3OH$	1:4	15	400–4000	1	0.14	1.33	1	3, 8
$CO:CH_3OH$	1:9	15	400–4000	1	0.11	1.33	1	2, 8
$CO:H_2O$	1:10	10	455–4555	1	0.13	1.32	2	4, 6
CO	Pure	10	2000–2200	1	0.09	1.30	2	4, 5, 6
$CO:O_2:N_2:CO_2$	1:0.5:0.25:0.32	10	570–4685	1	0.097	1.30	2	
$CO:O_2:N_2:CO_2$	1:5:1:0.5	12	2065–2228	0.9	0.185	1.24	3[a]	

References: (1) Cuppen et al. (2011); (2) Ehrenfreund et al. (1996); (3) Elsila et al. (1997).
Note. [a]Data can be found in http://www.astrochem.org/data/COMix.php

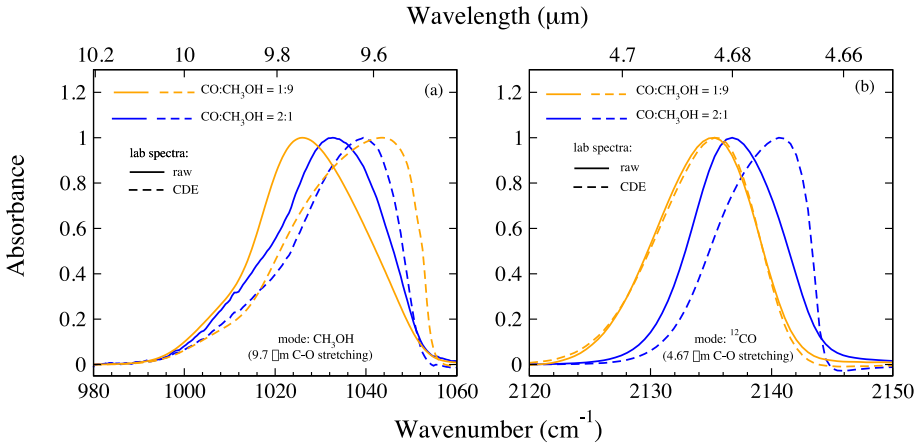

Figure 2. Laboratory spectra. Mixtures shown here are $CO:CH_3OH = 2:1$ (blue) and 1:9 (orange) in both panels. Raw laboratory spectra are represented by solid lines, while dashed lines represent grain shape corrected spectra (CDE). Panel (a) shows the 1026 cm^{-1} methanol band and ^{12}CO band is shown in panel (b). The spectra are all normalized. The relevant molecule and its correspondent mode are highlighted in each panel. (A colour version of this figure is available in the online version.)

2976, and 2828 cm^{-1} methanol features, and a band strength of 1.1×10^{-17} cm $molec^{-1}$ (Gerakines et al. 1995) for the CO stretch mode. The values of n_0 and the estimated thickness are noted in Table 1. We estimate the ice densities by a combination of the pure methanol density (Galvez et al. 2009) and pure CO density (Loeffler et al. 2005). For H_2O-rich ices, we use the band strength of 1.2×10^{-17} (Gerakines et al. 1995) for the 1660 cm^{-1} water O–H bend integrated over the 1250–2000 cm^{-1} range. No baseline subtraction of the raw laboratory spectra is performed until this stage.

4.2 Grain shape corrections

The new spectrum which takes grain shape corrections into account can be found by calculating the average absorption cross-section over the distribution of ellipsoidal homogeneous shapes and over all orientation in space, i.e. $\langle\langle C_{\rm abs}\rangle\rangle$. Here we use a CDE model (Bohren & Huffman 1983). The new spectrum is then calculated as follows:

$$\frac{\langle\langle C_{\rm abs}\rangle\rangle}{V} = \nu {\rm Im}\left\{\frac{2\varepsilon}{\varepsilon - 1}\left[\ln|\varepsilon| + i\arg(\varepsilon)\right]\right\}, \quad (1)$$

where V is the volume of the ellipsoid, ν is the wavenumber, and ε is the dielectric function (which is related with the optical constants n and k by $\varepsilon = n^2 - k^2 + i2nk$), and $\arg(\varepsilon)$ is the argument of ε. The effect of applying grain shape corrections to the laboratory spectra is shown in Fig. 2.

The raw and grain shape corrected laboratory spectra of two $CO:CH_3OH$ mixture ratios are shown for two different bands: 1026 cm^{-1}, dominated by methanol, and 2140 cm^{-1}, dominated by CO. For clarity, the spectra are normalized to the maximum of each band. The main effect of grain shape corrections on the laboratory spectra is a shift of peak position towards higher wavenumbers. As expected, this effect is more pronounced on the bands that correspond to the species that dominate the mixture.

4.3 Ice components and constraints

The observed CO profile shows deep and narrow lines which are caused by gas-phase CO, as shown in Fig. 1. In order to fit the 2140 cm^{-1} ^{12}CO band, we first remove the gas-phase peaks from the observed spectra so that the fit can be performed along the solid phase only. All grain shape corrected spectra are then baseline subtracted in a linear piece-wise fashion. A linear least-squares fit is then performed between different mixtures in order to fit the ^{12}CO band. To reproduce the polar component, we use the following mixtures: $CO:CH_3OH = 2:1$, 1:1, 1:2, 1:4 and 1:9, as well as $CO:H_2O = 1:10$. The blue component is less well understood and not many appropriate laboratory spectra are available. Therefore, a Gaussian with full width at half-maximum =3 and centre at 2143.7 μm is used to account for the blue component (Pontoppidan et al. 2003).

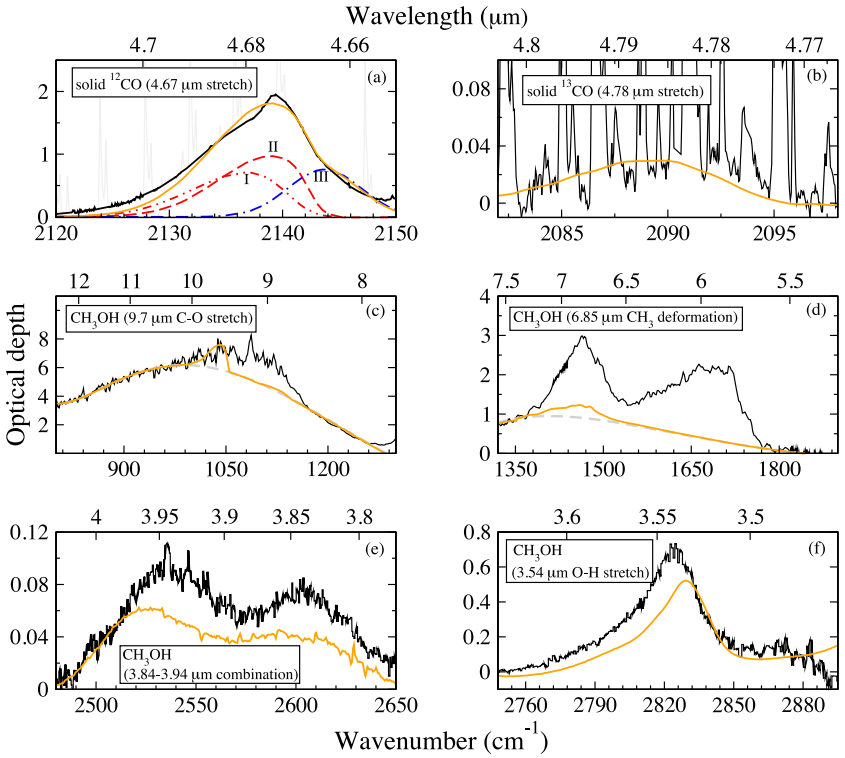

Figure 3. Observed spectra of AFGL 7009S and the resulting fit derived from the linear combination of a specific set of mixtures. In all panels, the orange continuous line represents the resulting fit. Panel (a) shows the observed ^{12}CO band (Keck spectrum, solid phase in black, and gas phase in light grey), and the mixtures CO:CH$_3$OH = 1:4 (I, double-dot dashed red line), CO:CH$_3$OH = 1:1 (II, dashed red line), and Gaussian (III, dot–dashed blue line). All mixtures are grain shape corrected (CDE). Panel (b) shows the ^{13}CO band (Keck spectrum, solid and gas phase in black). Panel (c) shows the 1026 cm^{-1} methanol band (ISO spectrum) with a fourth-order polynomial fit (dashed grey line) to subtract the silicate contribution. The same in panel (d), but for the 1460 cm^{-1} methanol band. Panels (e) and (f) show the United Kingdom Infrared Telescope spectra of 2540–2600 and 2828 cm^{-1} absorption methanol bands, respectively. The relevant molecule and its correspondent mode are highlighted inside boxes. (A colour version of this figure is available in the online version.)

When fitting the ^{12}CO band with mixtures containing methanol, we want to ensure that this will not produce an overshoot at some other spectral range with a methanol feature, even if the ^{12}CO is fitted well. The same holds for water-containing mixtures for the water bending mode. For CH$_3$OH, these bands are the C–O stretching mode at 1026 cm^{-1}, the CH$_3$ deformation band at 1455 cm^{-1}, the C–H stretching band at 2828 cm^{-1}, and the 2538–2604 cm^{-1} combination modes. The C–O stretching band is blended with silicate and the CH$_3$ deformation band is blended with other species. As suggested by Bottinelli et al. (2010), a fourth-order polynomial was used to account for the local continuum due to silicates. For the 1026 cm^{-1} band, the polynomial was fitted to the points 800–960 cm^{-1}, 1083–1087 cm^{-1}, and 1163–1282 cm^{-1}. For the 1460 cm^{-1} band, the points within the 1280–1284 cm^{-1}, 1333–1370 cm^{-1}, and 1785–2000 cm^{-1} ranges are used. The combination of these intervals produces continuum profiles that look reasonable upon visual inspection. When water containing mixtures are used, we take the O–H bend at 1660 cm^{-1} as constraint. This feature is also blended with silicates. Therefore, the continuum was subtracted by using a fourth-order polynomial fitted to the same points as for the 1460 cm^{-1} band.

The ^{13}CO band is also an important constraint. The ^{12}CO/^{13}CO ratio from the laboratory mixtures can be different from the ratio found in space. Therefore, the fitting of both bands is performed separately. To fit the ^{13}CO we use the same procedure and mixtures as used to fit the ^{12}CO band. However, for the ^{13}CO band, the contamination by gas-phase CO is stronger than for the ^{12}CO band, enough to preclude distinction of all gas-phase peaks in order to remove them from the observed spectra. Therefore, the fit is performed normally for both solid- and gas-phase ^{13}CO and then adjusted by visual inspection until a reasonable final fit is reached.

5 RESULTS

This section presents the resulting fits for the ^{12}CO, ^{13}CO, CH$_3$OH, and H$_2$O bands observed in the YSOs AFGL 7009S and L1489 IRS spectra. Only the best fits are shown.

5.1 AFGL 7009S: a high-mass YSO

The observed spectra of AFGL 7009S are shown in Fig. 1, including the first detection of solid ^{13}CO in the 'polar' phase. High-quality Keck observation of ^{12}CO and ^{13}CO bands is presented in panel 'a' as well as in panel 'b', respectively. Panel 'a' also presents a lower resolution ISO spectrum which shows how the ^{12}CO band overlaps with a XCN band at shorter wavelengths. Fig. 3 shows a zoom of the same spectra with the gas-phase lines subtracted along with the fit of these bands for AFGL 7009S, which is the result of a linear combination of the mixtures CO:CH$_3$OH = 1:1, 1:4, and the Gaussian described before. The first two mixtures account for the red component, while the Gaussian accounts for the blue component. The contributions of these components are shown in detail in Fig. 3(a). We can see that a linear combination of these mixtures provides a satisfactory fit to the ^{12}CO and ^{13}CO bands and no overshooting

Table 2. CO and methanol column densities.

Source	Molecule	Band position (cm^{-1})	$\int \tau d\tau$ (cm^{-1})	A^* (cm/molec)	N (molec cm^{-2})
AFGL 7009S	CO	2140	21.51	1.1 (−17)	1.95(18)
	CH_3OH	1026	54.40	1.5 (−17)	3.63(18)
L1489 IRS	CO	2140	7.66	1.1 (−17)	6.97(17)
	CH_3OH	1026	10.82	1.5 (−17)	7.21(17)

$a(-b) = a \times 10^{-b}$.
*References: A(CO) taken from Gerakines et al. (1995), and A(CH_3OH) taken from Grim et al. (1991).

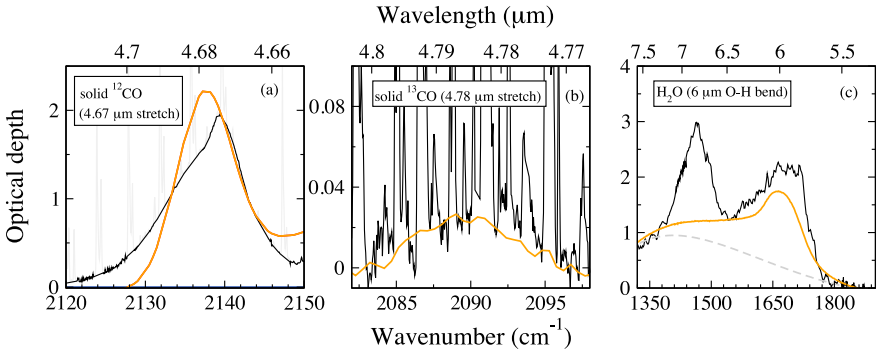

Figure 4. (a) Observed ^{12}CO band (Keck spectrum, solid phase in black, and removed gas phase in light grey), (b) observed ^{13}CO (Keck spectrum, gas and solid phase in black), and (c) 1660 cm^{-1} water band of AFGL 7009S (ISO spectrum, black). In all panels, orange line is the fit resulting from the linear combination of the following mixtures: CO:H_2O = 1:10 (T=10 K; unannealed), pure CO, and Gaussian. All mixtures are corrected for CDE grain shapes. With this set of mixtures, the contributions of pure CO and the Gaussian are null. Grey dashed line in panel (c) represents the continuum subtraction. (A colour version of this figure is available in the online version.)

appears in the other bands (Figs 3 c–f). Finally, we derived the solid CO and methanol column densities by dividing the integrated optical depth by the appropriate band strength A (see references in Section 4.1). We then obtained N(CO) = 1.95 × 10^{18} molec cm^{-2} and N(CH_3OH) = 3.63 × 10^{18} molec cm^{-2}. These findings are in agreement with previous studies, e.g. Dartois et al. (1999) and Boogert et al. (2008). Our results lead to N(CH_3OH)/N(CO) ≈ 1.85, which shows that methanol is the second most abundant species towards AFGL 7009S (Dartois et al. 1999). The column density values are summarized in Table 2.

As already discussed in Section 1, CO mixed with H_2O has been argued to be the carrier of the red component of the ^{12}CO band. Therefore, we also investigated the fit resulting from such a mixture. Fig. 4 shows the results of the application of a CO:H_2O = 1:10 mixture to fit the red component. A pure CO spectrum is used to fit the middle component, and the Gaussian to fit the blue component. Here, the constraint is the 1660 cm^{-1} water band due to the OH-bend mode. In order to get an appreciable width of the CO band, a strong dilution factor is required, but the spectrum is no longer sensitive to the exact ratio. As can be observed, the overall fit is much poorer, since both position and width are not correctly reproduced, in both short and long wavelengths. The blue component of the ^{12}CO band is overshot, which can be explained by the fact that CO mixed with H_2O produces a shoulder at 2152 cm^{-1} as described above, and the red component is not reproduced at all. Here we cannot see the shoulder at 2152 cm^{-1} present in the spectra of CO:H_2O mixtures because the fit is correlated with the Keck spectrum, which does not cover this band. Although the presence of a shoulder is an important constraint against CO:H_2O mixtures, a conclusion hardly can be extracted here because the short wavelength of the ^{12}CO band overlaps with the long wavelength of the XCN band. This overlap brings extra uncertainties on the presence of CO and H_2O mixtures towards AFGL 7009S. However, another constraint exists in the long wavelength side of the CO feature. Since the fit there is extremely poor, this is an extra and stronger argument against CO:H_2O mixtures than the presence of a shoulder at 2152 cm^{-1}. Thus, comparing results presented in Figs 3 and 4, we conclude that CO mixed with CH_3OH produces better fits for the CO bands towards the AFGL 7009S source.

5.2 L1489 IRS: a low-mass YSO

The present section reports results for the source L1489 IRS. It is known that low-mass YSOs also show methanol bands in their spectra (Boogert et al. 2008), although generally with much lower abundance. The same methanol bands described in the previous section are used here as constraints for the L1489 IRS source. Water-containing mixture is also used to fit the ^{12}CO and ^{13}CO bands. The observed spectrum of L1489 IRS is shown in Fig. 1. The observed ^{12}CO and ^{13}CO absorption bands are shown in panels 'a' and 'c', respectively. A zoom of the spectrum is reproduced in Figs 5(a) and (b). Middle and bottom panels show the four methanol bands used as constraints. The mixtures used here are: CO:CH_3OH = 1:1, CO:CH_3OH = 1:2, pure CO and a Gaussian with the same full width at half-maximum and position as used for AFGL 7009S. The ^{12}CO band is fitted well with this set of mixtures and no overshooting is observed at the other bands. It is necessary to use lower CH_3OH/CO ratios to fit L1489 IRS than the previous source, which reflects the fact that low-mass YSOs have a lower methanol content than high-mass YSOs. The contamination by gas-phase CO is so strong in the ^{13}CO band that we cannot expect a good fit at this band (Fig. 5b). The 1026 and 1460 cm^{-1} are also satisfactory, since no overshooting is observed. The spectrum of L1489 IRS shows that no feature is observed around 2538–2604 cm^{-1} (Figs 5 e and f). For this source, we

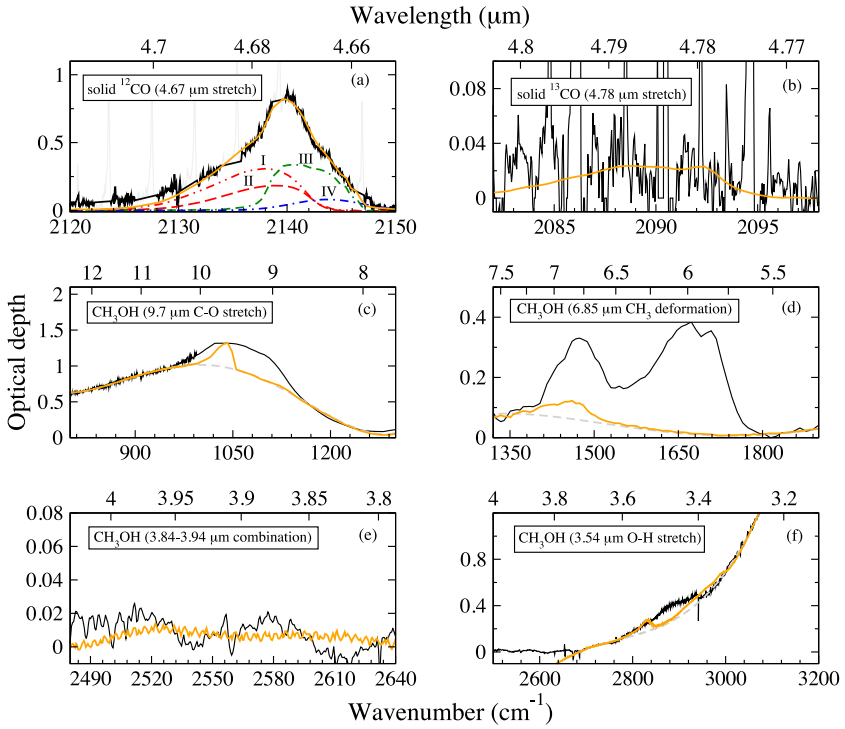

Figure 5. Observed spectra of L1489 IRS and the resulting fit derived from the linear combination of a specific set of mixtures. In all panels, the orange line represents the resulting fit. Panel (a) shows the observed ^{12}CO band (Keck spectrum, solid phase in black, and gas phase in light grey) and the contribution of the mixtures CO:CH_3OH = 1:2 (I, double dot–dashed red line), CO:CH_3OH = 1:1 (II, dashed red line), pure CO (III, dot–double dashed green line), and Gaussian (IV, dot–dashed blue line). All mixtures are corrected for CDE grain shapes. Panel (b) shows the observed ^{13}CO band (Keck spectrum, solid and gas phase in black), the region where absorption by ^{13}CO ice is expected, although no detection is claimed. Panel (c) shows the 1026 cm^{-1} methanol band (ISO spectrum) with a fourth order polynomial fit (dashed grey line) to subtract the silicate contribution. The same in panel (d), but for the 1460 cm^{-1} methanol band. Panels (e) and (f) show the ISO spectra of 2540–2600 and 2828 cm^{-1} absorption methanol bands, respectively. The relevant molecule and its correspondent mode are highlighted inside boxes. (A colour version of this figure is available in the online version.)

found $N(CO) = 6.97 \times 10^{17}$, and $N(CH_3OH) = 7.21 \times 10^{17}$ molec cm^{-2}, following the same procedure as described in Section 5.1 for the previous source. Our value of N(CO) is in agreement with Boogert et al. (2002a), but our $N(CH_3OH)$ value, however, is higher compared to Boogert et al. (2008) by a factor of at least 2.4. According to our results, the $N(CH_3OH)/N(CO)$ is close to unity, which means that both species have similar abundances towards L1489 IRS. Values of column densities are summarized in Table 2. We will come back to possible origins of this discrepancy in the next section.

Fig. 6 shows the fit using the 1660 cm^{-1} water band as a constraint for the observed ^{12}CO and ^{13}CO absorption bands. The mixtures used here are as follows: CO:H_2O = 1:10, pure CO, and Gaussian. Although the resulting fit is in better agreement with the observed L1489 IRS spectrum than it is for AFGL 7009S when the same set of mixtures is used, the fit is still poor. A mismatch is observed in the red component, and we can see clearly the shoulder produced by CO:H_2O mixtures at 2152 cm^{-1}. Therefore, we reinforce the fact that CO:H_2O mixtures do not produce the red component of the ^{12}CO band.

6 DISCUSSION AND CONCLUDING REMARKS

We have put our hypothesis that the red component in spectra of solid CO is caused by CO mixed with CH_3OH further to the test by looking at two specific sources: AFGL 7009S, a high-mass YSO, and L1489 IRS, a low-mass YSO. We applied corrections for grain shape effects and used different methanol bands to constrain the mixtures used to fit the ^{12}CO band. Water-containing mixtures were also tested.

We want to stress that the mixtures used to fit the red component represent the ratio localized in the mantles, which does not necessarily represent the ratios along the line of sight. The high spectral resolution of the observed spectra allowed us to confirm that unannealed spectra of water-containing mixtures cannot be reconciled with the polar CO component in both the high- and low-mass source studied.

Here, we used CO:CH_3OH = 1:1 and 1:4 for AFGL 7009S, and 1:1 and 1:2 for L1489 IRS to fit the red component. However, this does not mean that the grain mantles in these sources contain two distinct layers of exactly that composition (see Fig. 7 top-left). As can be seen in Fig. 8, spectra of ices of two different compositions, in this case CO:CH_3OH = 1:1 and 1:9, can be used to construct spectra of intermediate mixtures, in this case CO:CH_3OH = 1:2 and 1:4. We can observe that CO:CH_3OH = 1:2 and 1:4 ratios can be reproduced almost perfectly by a linear combination of the raw and grain shape corrected spectra of CO:CH_3OH = 1:1 and 1:9 ratios. However, this breaks down when using CO:CH_3OH = 2:1 instead of 1:1 ratios to fit the other mixtures since grain shape effects start to dominate (although this is not shown here). This indicates that mantles could also consist of one homogeneous intermediate layer (top right of Fig. 7). We think, however, that it is more likely that a gradient of different ice compositions exists (bottom left Fig. 7). This is in line with kinetic Monte Carlo simulations of methanol

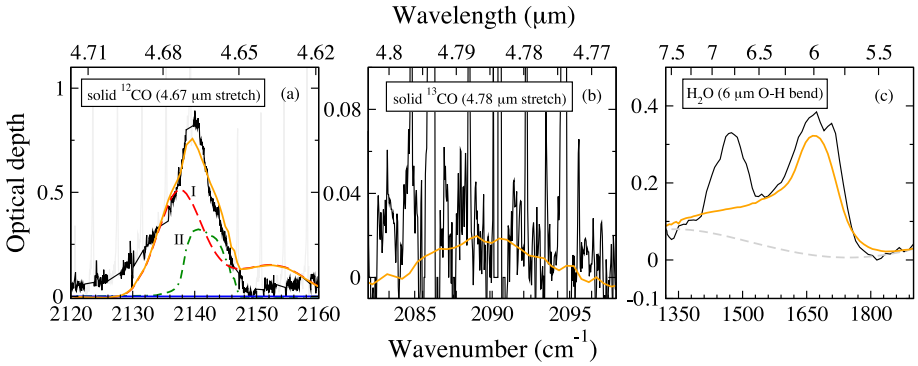

Figure 6. Same as for Fig. 4 but now for L1489 IRS. Panel (a) shows the contributions of CO:H_2O = 1:10 (T=10 K; unannealed) (I, dashed red line), and pure CO (II, dot–double dashed green line). The contribution of Gaussian is null. All mixtures are corrected for CDE grain shapes. (A colour version of this figure is available in the online version.)

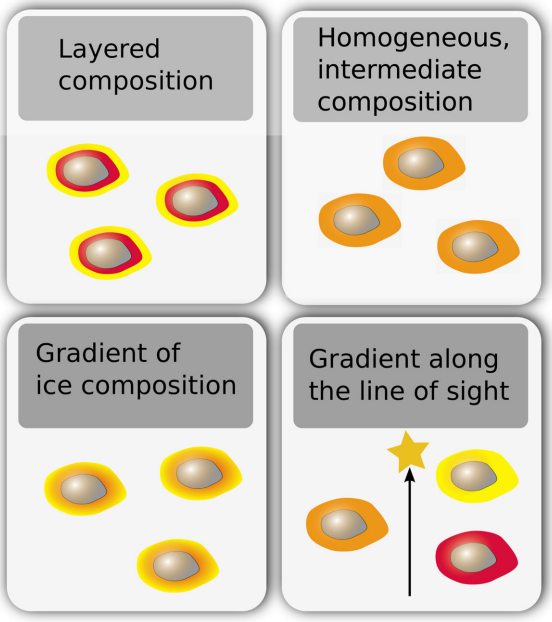

Figure 7. Possible interpretation of mantle structure of astrophysical ices. Top left panel: the ice mantle is composed by an intermediary composition distributed homogeneously. Top right panel: traditional view of ice mantles, where different layers of specific composition each take place. Bottom left panel: mantles are composed by a gradient of ice composition. Bottom right: mantles of different composition distributed along the line of sight. (A colour version of this figure is available in the online version.)

formation in dense clouds (Cuppen et al. 2009) where a gradient was found as well, caused by a changing CO/H ratio in gas phase during CO freeze-out. Although we cannot say exactly which range exists in the mantles, our results indicate that CO/CH_3OH ratios are limited, so that one should not expect extremes like CO:CH_3OH = 2:1 or 1:9 ratios to be present in the ice mantles. Another interpretation is that mantles change in composition along the line of sight (bottom right Fig. 7). Most likely it is a combination of both. Considering the evolution of grain surface mantles, it can indeed be easily explained why CO is in a CH_3OH rather than a H_2O environment. Observational studies show that H_2O freezes out at much lower extinctions (Whittet et al. 2001; Chiar et al. 2011; Boogert et al. 2013; Whittet et al. 2013) than CO, which needs a higher density to freeze out (Chiar et al. 1994). Methanol forms at even higher extinction as shown by ice observations (Boogert et al. 2011; Chiar et al. 2011; Whittet et al. 2011), which is consistent with the picture that a relatively high density is needed to efficiently convert CO into CH_3OH (Cuppen et al. 2009; Boogert, Gerakines & Whittet 2015).

For the sources used here we can reproduce the ^{12}CO band well by using a linear combination of different mixtures containing methanol to represent the red component. Moreover, the high-mass source required mixtures with a higher content of methanol than the low-mass source, in agreement with the CH_3OH abundances. According to our results, the column of CH_3OH of AFGL 7009S is in agreement with previous studies, while the same column is overestimated for L1489 IRS.

Due to the grain shape corrections, we need to include mixtures with large concentration of CH_3OH. For spectra with ratios $CH_3OH:CO \leq 1$, spectra of intermediate mixtures can no longer be obtained by a linear combination of two extreme mixtures as was done for $CH_3OH:CO \geq 1$ in Fig. 8. Moreover, the effect of CDE is a shift of the laboratory spectrum with several wavenumbers. Since we work with binary mixtures, the methanol serves two purposes: to change the band profile of the laboratory spectra and to change the effect of the grain shape corrections by changing the dilution ratio. Adding multiple components or changing the grain shape CDE model could make the amount of CH_3OH needed for a reasonable fit less severe. Moreover, it might also explain the minor disagreement that can be observed at short wavenumbers (see Figs 3 a and 5a).

The CDE model assumes only a single and homogeneous ice layer instead of a gradient as we suggest. Moreover, we ignore the presence of intermediate species, such as H_2CO, in the CO:CH_3OH mixtures. It is known from laboratory experiments that CH_3OH is produced via hydrogenation of CO in interstellar ices (Watanabe et al. 2004; Fuchs et al. 2009), which leads to intermediate species such as H_2CO. This would be more important for low-mass YSO, since these sources are less processed due to their lower temperature and density. Therefore, the conversion of the CO content into methanol takes longer, which means that the abundance of intermediate species might be higher than for high-mass YSO. However, as far as we are aware, there are no CO:H_2CO:CH_3OH mixtures currently available to put this hypothesis to test. Therefore, the effect of grain shape correction in the laboratory spectra of CO:H_2CO:CH_3OH mixtures is unknown. Nevertheless,

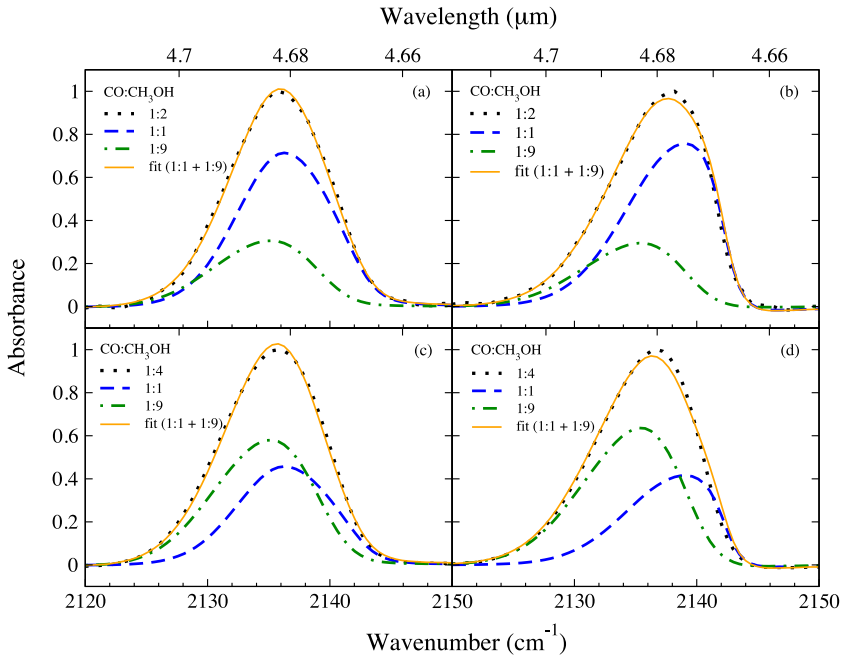

Figure 8. Linear combination of two different $CO:CH_3OH$ mixtures to fit a third one. The fit for the ^{12}CO band is shown in all panels. Left-hand panels show raw laboratory spectra while right-hand panels show the spectra after grain shape corrections (CDE). Panels (a) and (b) show $CO:CH_3OH = 1:1$ (dashed blue line), and 1:9 (dot–dashed green line) ratios fitting 1:2 ratio (dot black line). The same in panels (c) and (d), but now the fitting mixture is the $CO:CH_3OH = 1:4$ ratio (dot black line). (A colour version of this figure is available in the online version.)

based on the good fit shown by our results especially for AFGL 7009S, we reinforce that methanol is the more likely species to be mixed with CO and compose the red component of the ^{12}CO band.

Finally, we like to make a few considerations on the blue component. The apolar blue component has been argued to be caused by pure CO or CO mixed with CO_2. However, as pointed out by Boogert et al. (2002b), in astrophysical environments it is more likely that CO is mixed with other species as well, such as N_2 and O_2. Therefore, we tested the following mixtures: one O_2-rich ($CO:O_2:N_2:CO_2 = 1:5:1:0.5$), and one CO-rich ($CO:O_2:N_2:CO_2 = 1:0.5:0.25:0.32$). These mixtures are used here to test possible dependency on the choice of the blue component. The observed ^{13}CO and ^{12}CO absorption bands and the methanol features were fitted using also these two mixtures. CO- or O_2-rich mixtures do not exert a strong influence on the final fit: the red component is not affected by the blue component. Moreover, the inclusion of a pure CO component does not improve the quality of the fit substantially for AFGL 7009S. The columns derived from all combinations of fits are similar, although the $N(CO)/N(CH_3OH)$ ratio can be approximately 10 per cent higher than the ratio from standard mixtures, but still in agreement with previous studies for AFGL 7009S. For the L1489 IRS source, the CO and CH_3OH columns are all similar and the $N(CO)/N(CH_3OH)$ ratios are all close to unity. In conclusion, the red components of both AFGL 7009S and L1489 IRS are not affected by the choice of the blue component. However, for L1489 IRS, a pure CO component is necessary to have acceptable fits.

We can summarize the main conclusions as follows.

(1) Unannealed water-containing mixtures do not reproduce the ^{12}CO band of both high- and low-mass YSOs.

(2) The red component of the ^{12}CO band can be reproduced by $CO:CH_3OH$ mixtures. The previous conclusion that the mantle is stratified still holds.

(3) A gradient of different ratios of $CO:CH_3OH$ mixtures might exist in the grain mantles.

(4) The methanol constraints put limits on the CO/CH_3OH ratio, so that values of $CO:CH_3OH$ might not differ much from the 1:1 to 1:4 range.

(5) The spectrum of high-mass YSOs requires a higher content of methanol than the low-mass YSOs to reproduce the red component of the ^{12}CO band;

Although the present work shows that the red component of observed ^{12}CO band of YSO can be reproduced by $CO:CH_3OH$ mixtures, we want to stress that other combinations of ice mixtures might also produce equally good fits. However, our hypotheses are theoretically well-motivated and appear to be consistent with observations. Nevertheless, future work might take into account laboratory spectra of $CO:H_2CO:CH_3OH$ to provide a more complete picture of the chemical content of ice mantles. Moreover, the CDE model is not completely accurate, and might fail specially in the case of mantle stratification. Therefore, future work should also test other grain shape models. Ultimately, other mixtures, including follow-up experiments with UV photolysis and thermal processing, and different grain shape models should be tested in a bigger sample of YSO to allow a statistical analysis of the results presented here. This could shine a new light on the comprehension of the evolution of astrophysical ices and their role in the evolution of YSOs.

ACKNOWLEDGEMENTS

EMP and HMC acknowledge the European Research Council (ERC-2010-StG, Grant Agreement no. 259510-KISMOL) for financial support. HMC is grateful for support from the VIDI research program 700.10.427, which is financed by The Netherlands Organization for Scientific Research (NWO). SI acknowledges financial support from the Royal Society. GAB gratefully

acknowledges support from the NASA Origins of Solar Systems and NSF AAG programs.

REFERENCES

Acharyya K., Fuchs G. W., Fraser H. J., van Dishoeck E. F., Linnartz H., 2007, A&A, 466, 1005
Bohren C. F., Huffman D. R., 1983, Absorption and Scattering of Light by Small Particles. John Wiley & Sons, New York
Boogert A. C. A., Hogerheijde M. R., Blake G. A., 2002a, ApJ, 568, 761
Boogert A. C. A., Blake G. A., Tielens A. G. G. M., 2002b, ApJ, 577, 271
Boogert A. C. A. et al., 2008, ApJ, 678, 985
Boogert A. C. A. et al., 2011, ApJ, 729, 92
Boogert A. C. A., Chiar J. E., Knez C., Öberg K. I., Mundy L. G., Pendleton Y. J., Tielens A. G. G. M., van Dishoeck E. F., 2013, ApJ, 777, 73
Boogert A. C. A., Gerakines P. A., Whittet D. C. B., 2015, ARA&A, 53, 541
Bottinelli S. et al., 2010, ApJ, 718, 1100
Chiar J. E., Adamson A. J., Kerr T. H., Whittet D. C. B., 1994, ApJ, 426, 240
Chiar J. E. et al., 2011, ApJ, 731, 9
Cuppen H. M., van Dishoeck E. F., Herbst E., Tielens A. G. G. M., 2009, A&A, 508, 275
Cuppen H. M., Penteado E. M., Isokoski K., van der Marel N., Linnartz H., 2011, MNRAS, 417, 2809
Dartois E., Schutte W., Geballe T. R., Demyk K., Ehrenfreund P., D'Hendecourt L., 1999, A&A, 342, L32
Ehrenfreund P., Boogert A. C. A., Gerakines P. A., Jansen D. J., Schutte W. A., Tielens A. G. G. M., van Dishoeck E. F., 1996, A&A, 315, L341
Ehrenfreund P., Boogert A. C. A., Gerakines P. A., Tielens A. G. G. M., van Dishoeck E. F., 1997, A&A, 328, 649
Elsila J., Allamandola L. J., Sandford S. A., 1997, ApJ, 479, 818
Fraser H. J., Collings M. P., Dever J. W., McCoustra M. R. S., 2004, MNRAS, 353, 59
Fuchs G. W., Cuppen H. M., Ioppolo S., Romanzin C., Bisschop S. E., Andersson S., van Dishoeck E. F., Linnartz H., 2009, A&A, 505, 629
Galvez O., Mate B., Martin-Llorente B., Herrero V., Escribano R., 2009, J. Chem. Phys., 113, 33213329
Gerakines P. A., Schutte W. A., Greenberg J. M., van Dishoeck E. F., 1995, A&A, 296, 810
Grim R. J. A., Baas F., Greenberg J. M., Geballe T. R., Schutte W., 1991, A&A, 243, 473
Hudgins D. M., Sandford S. A., Allamandola L. J., Tielens A. G. G. M., 1993, ApJS, 86, 713
Loeffler M. J., Baratta G. A., Palumbo M. E., Strazzulla G., Baragiola R. A., 2005, A&A, 435, 587
McLean I. S. et al., 1998, in Proc. SPIE 3354, Infrared Astronomical Instrumentation. SPIE, p. 566
Öberg K. I., van Broekhuizen F., Fraser H. J., Bisschop S. E., van Dishoeck E. F., Schlemmer S., 2005, ApJ, 621, L33
Pontoppidan K. M. et al., 2003, A&A, 408, 981
Sandford S. A., Allamandola L. J., Tielens A. G. G. M., Valero G. J., 1988, ApJ, 329, 498
Schmitt B., Greenberg J. M., Grim R. J. A., 1989, ApJ, 340, L33
Tielens A. G. G. M., Tokunaga A. T., Geballe T. R., Baas F., 1991, ApJ, 381, 181
Watanabe N., Nagaoka A., Shiraki T., Kouchi A., 2004, ApJ, 616, 638
Whittet D. C. B., Gerakines P. A., Hough J. H., Shenoy S. S., 2001, ApJ, 547, 872
Whittet D. C. B., Cook A. M., Herbst E., Chiar J. E., Shenoy S. S., 2011, ApJ, 742, 28
Whittet D. C. B., Poteet C. A., Chiar J. E., Pagani L., Bajaj V. M., Horne D., Shenoy S. S., Adamson A. J., 2013, ApJ, 774, 102

This paper has been typeset from a TEX/LATEX file prepared by the author.